A&A 413, 1073–1085 (2004)
DOI: 10.1051/0004-6361:20031590

Astronomy & Astrophysics

First stars IV. CS 29497–030: Evidence for operation of the *s*-process at very low metallicity⋆,⋆⋆

T. Sivarani[1], P. Bonifacio[1], P. Molaro[1], R. Cayrel[2], M. Spite[2], F. Spite[2], B. Plez[3], J. Andersen[4], B. Barbuy[5], T. C. Beers[6], E. Depagne[7], V. Hill[2], P. François[2], B. Nordström[8,4], and F. Primas[9]

[1] Istituto Nazionale di Astrofisica, Osservatorio Astronomico di Trieste, via Tiepolo 11, 34131 Trieste, Italy
e-mail: sivarani@ts.astro.it,molaro@ts.astro.it
[2] Observatoire de Paris-Meudon, GEPI, 92195 Meudon Cedex, France
e-mail: Vanessa.Hill@obspm.fr,Roger.Cayrel@obspm.fr,Monique.Spite@obspm.fr, Francois.Spite@obspm.fr,Patrick.Francois@obspm.fr
[3] GRAAL, Université de Montpellier II, 34095 Montpellier Cedex 05, France
e-mail: Bertrand.Plez@graal.univ-montp2.fr
[4] Astronomical Observatory, NBIfAFG, Juliane Maries Vej 30, 2100 Copenhagen, Denmark
e-mail: ja@astro.ku.dk
[5] IAG, Universidade de São Paulo, Departamento de Astronomia, CP 3386, 01060-970 São Paulo, Brazil
e-mail: barbuy@astro.iag.usp.br
[6] Department of Physics & Astronomy, Michigan State University, East Lansing, MI 48824, USA
e-mail: beers@pa.msu.edu
[7] European Southern Observatory, Casilla 19001, Santiago, Chile
e-mail: edepagne@eso.org
[8] Lund Observatory, Box 43, 221 00 Lund, Sweden
e-mail: birgitta@astro.lu.se
[9] European Southern Observatory (ESO), Karl-Schwarschild-Str. 2, 85749 Garching b. München, Germany
e-mail: fprimas@eso.org

Received 14 April 2003 / Accepted 1 October 2003

Abstract. We present an abundance analysis of the very metal-poor, carbon-enhanced star CS 29497–030. Our results indicate that this unusually hot turnoff star ($T_{\rm eff}$ = 6650 K, log g = 3.5) has a metallicity [Fe/H] = −2.8, and exhibits large overabundances of carbon ([C/Fe] = +2.38), nitrogen ([N/Fe] = +1.88), and oxygen ([O/Fe] = +1.67). This star also exhibits a large enhancement in its neutron-capture elements; the pattern follows that expected to arise from the *s*-process. In particular, the Pb abundance is found to be very high with respect to iron ([Pb/Fe] = +3.5), and also with respect to the second peak *s*-process elements (e.g., Ba, La, Ce, Nd), which fits into the newly introduced classification of lead (Pb) stars. The known spectroscopic binary status of this star, along with the observed *s*-process abundance pattern, suggest that it has accreted matter from a companion, which formerly was an Asymptotic Giant-Branch (AGB) star. In a preliminary analysis, we have also identified broad absorption lines of metallic species that suggest a large axial rotational velocity for this star, which may be the result of spin-up associated with the accretion of material from its previous AGB companion. In addition, this star is clearly depleted in the light element Li. When considered along with its rather high inferred temperature, these observations are consistent with the expected properties of a very low metallicity halo blue straggler.

Key words. nuclear reactions, nucleosynthesis, abundances – stars: abundances – stars: binary: spectroscopic – stars: individual: CS29497-030 – Galaxy: halo – Galaxy: abundances

1. Introduction

The two neutron-capture processes, the *slow* (*s*-process), and the *rapid* (*r*-process), occur under different physical conditions, and therefore are likely to arise in different astrophysical sites. In an early systematic study of elemental abundances in halo stars, Spite & Spite (1978) found that the neutron-capture elements Ba and Y were over-deficient with respect to iron, and that the barium abundance increased almost as fast as iron at

Send offprint requests to: P. Bonifacio,
e-mail: bonifaci@ts.astro.it

⋆ Based on observations made with the ESO Very Large Telescope at Paranal Observatory, Chile (program ID 165.N-0276(A)).

⋆⋆ Table 6 is only available in electronic form at http://www.edpsciences.org

low metallicity, suggesting a common origin in massive, short-lived stars. From this suggestion, Truran (1981) formulated the hypothesis that in the early Galaxy the neutron-capture elements were formed exclusively through the *r*-process, assumed to occur in core-collapse type II SNe; this idea is often referred to as the "*r*-only hypothesis." More recent observations of heavy-element abundance patterns in metal-poor stars have further supported this hypothesis (Gilroy et al. 1988; Burris et al. 2000 and references therein).

From the theoretical point of view, support for the "*r*-only hypothesis" comes from consideration of the timescales involved. The dominant site of the *s*-process is thought to be the Asymptotic Giant-Branch (AGB) phase in intermediate-mass stars (Busso et al. 1999, and references therein); by the time the first of these objects began polluting the interstellar medium with *s*-process elements, core-collapse SNe had already raised the mean metallicity of the early-Galaxy Inter-Stellar Medium (ISM) above [Fe/H] = −2.5. Previous stellar evolutionary models predicted that zero-metallicity stars would not undergo the thermally pulsing (TP) AGB phase (Fujimoto et al. 1984). Recently, however, Chieffi et al. (2001) showed that thermal pulses can in fact occur even in stars with no heavy elements. Although the environment might thus be appropriate, the lack of iron seeds in such stars is still thought to prevent the operation of the *s*-process, hence no neutron-capture elements are predicted to be produced by standard models of zero-metal TP-AGB stars (Abia et al. 2001; Chieffi et al. 2001; Siess et al. 2002; Iwamoto et al. 2003).

A growing body of observational evidence now suggests that, in contrast to the *r*-only hypothesis, the *s*-process could indeed operate even at very low metallicities. Whether or not it had a significant impact on the chemical evolution of neutron-capture elements throughout the early Galaxy is still an open question, as this depends on the Initial Mass Function of early-generation stars (Abia et al. 2001).

The large modern surveys for metal-poor stars (the HK survey Beers et al. 1985, 1992; Beers 1999a,b, and the Hamburg/ESO survey of Christlieb et al. 2000) have unveiled the existence of stars in which the abundances of neutron-capture elements are greatly enhanced, although there are some important differences between various classes of stars that exhibit this phenomenon, which can be broadly grouped as described below.

A few stars, such as CS 22892–052 (Sneden et al. 1994, 1996, 2000, 2003a), and CS 31082–001 (Cayrel et al. 2001; Hill et al. 2002), exhibit large enhancements of neutron-capture elements, including species that can only be synthesized through the *r*-process, such as Th and U. The observed abundance patterns of the heavy neutron-capture elements in these stars agree extremely well with a scaled solar-system *r*-process pattern, suggesting an *r*-process origin for all of them. These highly *r*-process-enhanced metal-poor stars appear to be extremely rare, with a frequency no greater than about 3% among giants with [Fe/H] < −2.5. It should be noted that although CS 22892–052 is enhanced in carbon ([C/Fe] ∼ +1.0; Sneden et al. 1994), it has been suggested (Aoki et al. 2002a) that the origin of the carbon in this star may not be causally connected to the origin of its *r*-process elements. CS 31082–001, on the other hand, is only mildly carbon-enhanced ([C/Fe] = +0.2; Hill et al. 2002).

Other very metal-poor stars in which the pattern of neutron-capture elements suggest an *s*-process enrichment are more common. Radial velocity variations have been observed in some (Norris et al. 1997; Preston & Sneden 2000; Aoki et al. 2002b), but not all of them (e.g., LP 706–7; Norris et al. 1997). In many of these *s*-process-enriched, metal-poor stars the element lead is detected and often considerably enhanced. This is not unexpected, since the operation of the *s*-process in a metal-poor star occurs with a high neutron-to-seed-nucleus ratio, thus favouring the formation of neutron-rich nuclei.

Lead was first detected in a metal-poor star by Cowan et al. (1996) in HD 126238, and later in HD 115444 and CS 22892–052 (Sneden et al. 1998, 2000). In our later discussion, for CS 22892–052 we adopt the Pb abundance derived from the optical lines, although it is very uncertain since the much stronger PbI 283.3 nm line has not been detected (Sneden et al. 2003a). We prefer this determination since the Pb abundance of CS 22892–052 estimated from the optical lines is consistent with that obtained in the small number of other known *r*-process-enhanced, metal-poor stars. In these three stars, Pb is attributed primarily to the *r*-process rather than to the *s*-process because of the large observed enhancements in other *r*-process elements such as Eu.

Lead of likely *s*-process origin was first detected in the carbon- and *s*-process-rich, metal-poor star LP 625–44 by Aoki et al. (2000), suggested by these authors to have originated from an AGB companion. Metal-poor stars with high Pb abundances relative to the second neutron-peak elements (Ba, La, Ce), as predicted by metal-poor AGB models (Goriely & Mowlavi 2000; Goriely & Siess 2001), were first discovered by van Eck et al. (2001). Subsequently, Pb has been detected in 21 more stars (Aoki et al. 2001; Travaglio et al. 2001; Aoki et al. 2002b; Johnson & Bolte 2002; Cohen et al. 2003; Lucatello et al. 2003; van Eck et al. 2003). These stars show a large range in [hs/Pb] ratio (hs representing second *s*-process-peak elements such as Ba, La, Ce and Nd). At present there appears to be no evidence for a correlation between [hs/Pb] ratio and metallicity of the lead stars.

All the *s*-process-enhanced stars also appear to be enhanced in carbon, hence one might speculate that they are analogs of the classical CH stars, all of which appear to be members of binary systems (McClure 1990, 1997). If this is universally true, the *s*-process elements and carbon have almost certainly been produced by a binary companion during its TP-AGB phase, and subsequently accreted onto the surviving companion star. To complete this (already complex) picture one must add that the reverse situation is not true; not all of the carbon-rich stars, which appear to represent as many as 15–25% of all stars with [Fe/H] < −2.5 (Beers et al. 1985, 1992; Beers 1999a,b; Christlieb et al. 2000), are also enhanced in their neutron-capture elements. In fact, there exist carbon-enhanced, metal-poor stars with no observed enhancements of neutron-capture elements at all (e.g., CS 22957-027, Norris et al. 1997; Bonifacio et al. 1998). Recently, Aoki et al. (2002b) have enlarged the number of such stars, suggesting that the phenomenon of mild carbon-enhancement without

accompanying neutron-capture enhancement amongst very metal-poor stars is not uncommon. In addition, there exists a class of extremely metal-poor stars (including CS 22949–037, Depagne et al. 2002, and CS 29498–043, Aoki et al. 2002a) that exhibit large excesses of N, O, Mg, and Si, in addition to C, with no apparent neutron-capture enhancement. It is thus not clear what relation, if any, exists between the carbon and neutron-capture-element enhancement phenomena.

In this paper we report a detailed high-resolution analysis of CS 29497-030, based on high-quality VLT/UVES spectra, which we show to be a very metal-poor star that exhibits enhanced abundances of neutron-capture elements with a pattern suggesting an *s*−process origin. CS 29497–030 was originally classified as A type by G. Preston from inspection of its objective prism image. The star was included as BHB candidate in the *UBV* survey of Preston et al. (1991a) but subsequently rejected as a BHB star on the basis of the two colour criterion by Preston et al. (1991b). It was subsequently identified as a high-gravity metal-deficient (BMP) star on the basis of its small $B-V$ and $U-B$ excess by Preston et al. (1994). As such it was also included in the spectroscopic survey of Wilhelm et al. (1999). In preparing our VLT observations T. C. Beers visually inspected the medium survey spectra of all the stars considered for possible follow-up at high resolution, and noticed a *G*-band of unusual strength compared to its hydrogen lines, which are typical of stars at or beyond the main-sequence TO, and thus marked it as a possibly carbon-rich star. Preston & Sneden (2000) included this star are part of a long-term radial velocity survey of BMP stars, and identified CS 29497–030 as a spectroscopic binary with a period of 342 days; the radial velocity curve is shown in Fig. 1.

As briefly reported earlier by our group (Sivarani et al. 2002), the most striking features of CS 29497–030, besides its very high C abundance, are its extremely high Pb abundance, which places CS 29497–30 amongst the most metal-poor lead stars yet identified, as well as its extremely high O abundance. CS 29497–30 is thus only slightly less enhanced in O than the extreme case of CS 22949–037, an extremely metal-poor giant with no evidence of binarity (Depagne et al. 2002).

2. Observations and data reduction

Our spectroscopic data were obtained at the VLT-Kuyen 8.2 m telescope, using the UVES spectrograph (Dekker et al. 2000) at a resolving power of $R = 43\,000$. The observations were made as a part of the Large Programme "First Stars"(165.N-0276; P.I. R. Cayrel); the log of observations is given in Table 1. The data were reduced using the UVES context within MIDAS, which includes bias subtraction, flat fielding, wavelength calibration, and merging of echelle orders. The continuum normalisation was performed with IRAF (using a cubic spline function) for the merged spectra. For a few lines that were either very weak or of particular interest, we have used the spectra of the individual orders without merging them. The Balmer lines of hydrogen were checked with both single-order and merged spectra. Equivalent-width measurements for unblended lines were accomplished by fitting gaussian profiles, using the genetic algorithm code described in François et al. (2003).

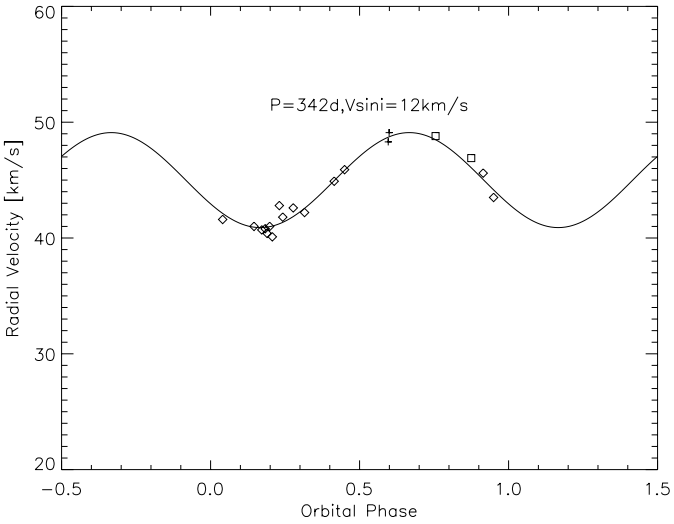

Fig. 1. The spectroscopic orbit of CS 29497-030 by Sneden et al. (2003a); the data by Preston & Sneden (2000) are shown by "◇", our data by "+" symbols.

Table 1. Log of observations.

Date	$t_{\rm exp}$(s)	$\lambda_{\rm c}$ (nm)	S/N^*	MJD–24000.5	v_R (km s^{-1})
19/10/2000	1800	396+850	75	51836.20	48.8
06/11/2001	1800	396+573	65	52219.17	46.9

* S/N at 440 nm.

Radial velocities were measured from the positions of unblended lines in the range 480–850 nm. Small instrumental shifts were corrected using the telluric absorption lines. As can be seen from inspection of Fig. 1, the new radial velocity data for CS 29497–030 provide tight constraints on the binary orbit, as they were obtained near one of the peaks in the velocity curve. The orbit calculated by Preston & Sneden (2000) is clearly confirmed by our new data.

3. Stellar parameters and analysis

CS 29497–030 was classified as an A V star by Wilhelm et al. (1999), indicating that it was thought to have a high surface gravity, at least as compared to the field horizontal-branch stars they were seeking to identify. They determined the stellar parameters given in Table 3, based on available *UBV* photometry and medium-resolution (∼1.5 Å) spectroscopy. Recently, Kinman & Castelli (2002) have derived temperatures based on the $V-J$, $V-H$, and $V-K$ colours, using 2MASS data and fitting the colours to Kurucz model predictions.

We have obtained new photometric data, $BVR_{\rm C}I_{\rm C}$ (the subscript "C" indicates the Cousins system) with the Danish 1.5 m telescope and DFOSC instrument (Beers et al. 2003). We estimate a color excess due to reddening of $E(B-V) = 0.016$ from the maps of Schlegel et al. (1998) and use the Alonso et al. (1996) calibrations to derive $T_{\rm eff}$ from the colours. The Alonso calibrations of $B-V$, $V-R$, $V-I$, $R-I$, and $V-K$ require colours in the Johnson system; calibrations of the IR colours,

$J-H$ and $J-K$, are in the TCS system (the native photometric system at the 1.54 m Carlos Sánchez telescope in Tenerife; Arribas & Martínez-Roger 1987).

To transform the colours from the Cousins to the Johnson system, we use the transformations derived by Bessell (1983), which for $R-I$ do not include the Paschen dip; Bessell points out that, as a result, these transformations are uncertain for $-0.05 \leq R-I \leq +0.3$. CS 29497–030 falls in this colour range, where the Paschen jump reaches a maximum. To obtain the $V-K$ colour in the Johnson system we transformed the 2MASS K magnitude to the Bessell & Brett (1988) homogenized system, using equations from Explanatory Supplement to the 2MASS All Sky Data Release (Cutri et al. 2003); note that this is a two-step calibration, 2MASS to CIT (the CIT system is described in Elias et al. 1982; Frogel et al. 1978), and then to the Bessell & Brett system. Therefore, the errors involved in the colour transformations must be added to those of the photometry.

To transform the 2MASS colours $J-H$ and $J-K$ onto the TCS system (Alonso et al. 1996) again required a two-step calibration, from 2MASS to CIT (Cutri et al. 2003), and then from CIT to TCS (Alonso et al. 1996). In Table 2, we list the errors in $T_{\rm eff}$ corresponding to the photometric errors.

The temperatures listed in Table 2 span a range of almost 1000 K. The $B-V$, $J-H$ and $J-K$ colours provide similar temperatures, while the $V-R$, $V-I$, and $V-K$ colours predict higher temperatures. The large errors in the temperatures derived from $J-H$ and $J-K$ are due to the very steep slope of the calibrations for the bluest stars. With this large spread in temperatures there is little point in averaging them. We therefore decided to rely on the Fe I excitation equilibrium, which implies $T_{\rm eff}$ = 6650 K, similar to the $T_{\rm eff}$ derived from the $B-V$, $J-H$, and $J-K$ colours. The wings of the Balmer lines are also consistent with this temperature. The presence of a CN molecular band in the spectra suggests that the temperatures cannot be as high as derived from the $R-I$, $V-I$, and $V-K$ colours. The only explanation we can offer for the large spread in effective temperatures derived from different colours is that the star has an anomalous spectral energy distribution, possibly due to its peculiar composition and/or its binary nature.

The FeI/FeII ionisation equilibrium has been used to fix the surface gravity of CS 29497–030. We point out that, with our adopted log g, balance is achieved, within the errors, also for TiI/TiII, MgI/MgII and MnI/MnII, although TiI and MgII are represented only by single lines. Dr. A. Korn kindly performed NLTE computations for the iron lines in order to check for NLTE effects on the derived gravity; he obtained log g(NLTE) = 3.65, confirming a rather low surface gravity for this star. Also, the observed $U-B$ colour of the star is compatible with this gravity.

The microturbulence was determined in the usual way, by requiring that the abundances derived from the Fe I lines be independent of the measured equivalent widths.

The model atmospheres (OSMARCS), spectrum synthesis code (TURBOSPEC by Plez), and the line data that we employed are the same as described in previous papers of this series (Hill et al. 2002; Depagne et al. 2002; François et al. 2003).

Table 2. Photometry of CS 29497−030.

Mag & colour		$T_{\rm eff}$	$\delta T_{\rm eff}$[a]
V	12.65 ± 0.002	···	···
$U-B$[b]	−0.14	···	···
$B-V$	0.299 ± 0.004	6680	20
$V-R_{\rm C}$	0.215 ± 0.003	6875	35
$V-I_{\rm C}$	0.440 ± 0.005	7016	25
$R-I_{\rm C}$	0.225 ± 0.008	7281	104
$V-K_{\rm 2Mass}$	0.905 ± 0.025	7153	59
$J-H_{\rm 2Mass}$	0.183 ± 0.038	6693	303
$J-K_{\rm 2Mass}$	0.217 ± 0.036	6563	257

[a] Change in $T_{\rm eff}$ for a $\pm 1\sigma$ change in the colour.
[b] Preston & Sneden (2000).

Table 3. Atmospheric parameters of CS 29497−030.

Reference	$T_{\rm eff}$	log g(cgs)	[Fe/H]	$\xi_{\rm t}$ km s^{-1}
1	7426	3.9	−2.5	···
2	7180	4.2	−2.0	···
3	7050	4.2	−2.16	1.75
4	6650	3.5	−2.7	2.0

(1) Wilhelm et al. (1999), (2) Kinman & Castelli (2002), (3) Sneden et al. (2003a) (4) Present Work.

4. Abundances

The derived elemental abundances for CS 29497–030 are listed in Table 4. The most striking features are the large overabundances of C, N, and O, relative to iron, and the large enhancement of all the *s*-process elements, among which Pb stands out with [Pb/Fe] = +3.5.

The chemical composition of CS 29497–030 was analysed earlier by Preston & Sneden (2000), who derived abundances for Fe, Mg, Ca, Sc, Ti, Cr, Mn, Sr, and Ba, and by Sneden et al. (2003), who derived in addition abundances for C, O and La, Nd, Eu and Pb. The overall abundance pattern derived by both the above analyses is similar to our own, with most elemental ratios showing agreement at a level of 0.2–0.3 dex. However, both obtain a significantly higher metallicity ([Fe/H] = –2.1, −2.16, respectively) than we do, probably due to the higher temperature adopted.

4.1. Carbon and nitrogen

We measured several CI and CH lines in our spectra. The CI lines, some of which are shown in Fig. 2, provide a C abundance that is about 0.3 dex higher than that derived from the CH lines. We suspect the difference could be due to NLTE effects in the CI lines, which have excitation potentials higher than 7.5 eV. We plan to perform NLTE computations in the near future to check on this possibility. Taking into account all the CI lines in the spectra, we obtain an abundance which is on average 0.1–0.3 dex higher than obtained from the CH lines. The ^{13}CH lines are very weak, so we could only derive a lower limit for the carbon isotope ratio: ^{12}C/^{13}C > 10.

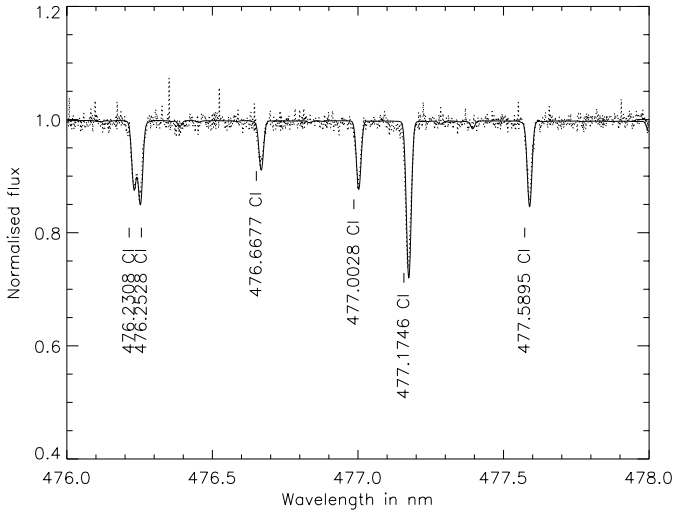

Fig. 2. Examples of the high-excitation CI lines observed in CS 29497–030. The solid line is the synthetic spectrum (for [O/Fe] = +1.67) computed with the fitted C abundance, which is 0.3 dex higher than what is derived from the CH lines. A probable cause of this discrepancy is NLTE effects, such as those that affect the OI 777 nm triplet.

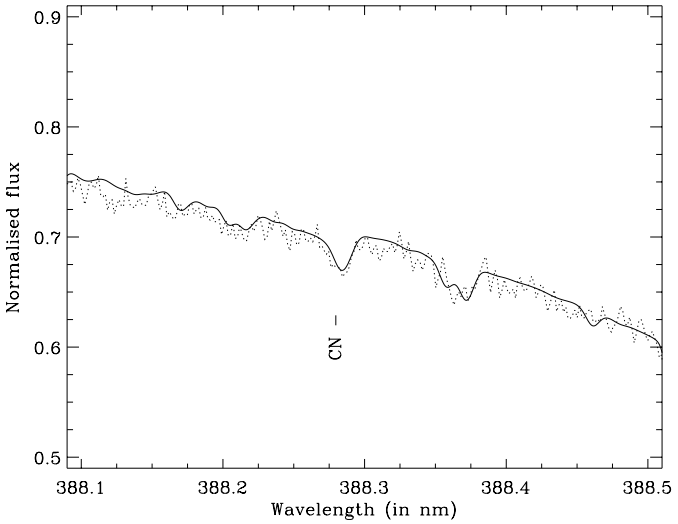

Fig. 3. The CN 388 nm bandhead. The dotted line represents the observed spectrum, while the solid line is the synthetic spectrum (for [O/Fe] = +1.67).

We have detected a very weak CN 388 nm bandhead, shown in Fig. 3, from which, assuming the C abundance derived from the CH lines, we derive [N/Fe] = +1.88.

We have checked the sensitivity of the derived carbon abundance to the adopted oxygen abundance by performing the analysis both with the high oxygen abundance derived from the OI 777.4 nm lines ([O/Fe] = +1.67), and for a much lower value ([O/Fe] = +0.5). We find no impact of these two widely different oxygen abundances on the derived carbon and nitrogen abundances.

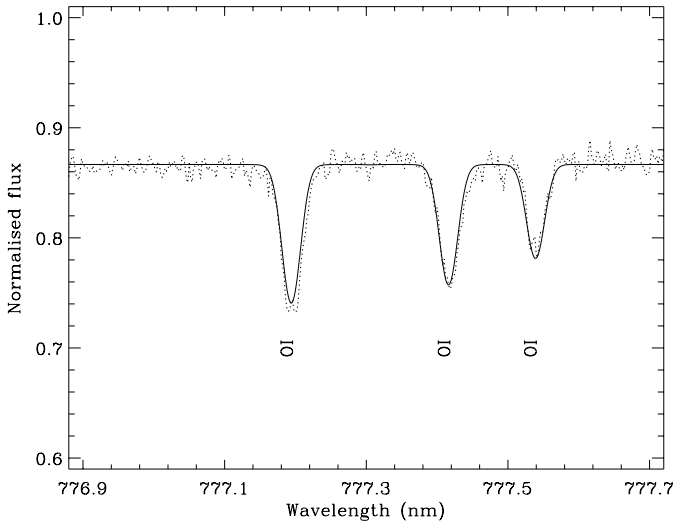

Fig. 4. The OI 777 nm triplet. In this and the following figures, the dotted line represents the observed spectrum, while the solid line is the synthetic spectrum.

4.2. The α elements

The oxygen abundance was derived from the OI 777.4 nm triplet shown in Fig. 4. The oxygen triplet is known to suffer from NLTE effects (Kiselman 1991; Takeda 1994; Gratton et al. 1999; Kiselman 2001). In order to correct for these effects we interpolated in Table 10 of Gratton et al. (1999) and found a correction of −0.09 dex; the NLTE corrected value is listed in Table 4. This oxygen abundance appears to be exceptionally high when compared to most other metal–poor stars (Depagne et al. 2002). Note that the high abundance derived from the OI 777.4 nm triplet is still consistent with the non-detection of the 615 nm OI triplet and 630 nm [OI] lines. There is always some concern in deriving abundances from the OI triplet. For example, for two giants in the LMC, Barbuy et al. (1994) report an overabundance of about 2.0 dex compared to the abundance derived from the 615.8 nm lines. On the other hand, there is at least one star, the very metal-poor subgiant BD +23° 3130, for which the oxygen abundance derived from the OI 777.4 nm triplet does agree with that derived from the [OI] 630 nm line and the OH UV lines (Cayrel et al. 2001; García López et al. 2001). In the comprehensive study of Carretta et al. (2000), oxygen abundances were derived both from permitted OI lines (the 616 nm triplet and the 777 nm triplet) and from the [OI] 630 nm line. There appears to be no systematic difference between these sets of abundances, as illustrated by their Fig. 3. In the case of CS 29497–030, the OI triplet is the only available oxygen indicator, hence our only choice is to take the derived oxygen abundance at face value, although with some caution.

Magnesium exhibits a "normal" overabundance of ∼0.5 dex above Fe. The MgII 448.1 nm doublet is detected, testifying to the relatively high effective temperature of this star. The derived abundance from the MgII doublet is only 0.1 dex higher than that derived from the MgI lines. Considering that the latter show a scatter of 0.2 dex, we consider the two abundances to be consistent.

We have detected a strong Si I line at 390.5 nm, and weak Si II lines at 385.6 nm and 386.2 nm; the derived abundances are [SiI/Fe] = −0.05 and [SiII/Fe] = +0.6, respectively. We have spectra taken on two different nights for this wavelength region; we find they are consistent with one another; therefore the problem should not originate in the data. The Si I line is saturated and sensitive to the adopted microturbulence, while the Si II lines are sensitive to log g. By adjusting the atmospheric parameters we obtain identical abundances ([Si/Fe] = +0.4) for Si I and Si II for a model with $T_{\rm eff}$ = 6750 K, log g = 3.0, $\xi_{\rm t}$ = 0.0 km s^{-1}. It is interesting to note that McWilliam et al. (1995) find a large dispersion in the Si abundance in a sample of 33 very metal-poor stars, based primarily on abundances estimated from the Si I 390.5 nm line. Also, there is a large difference seen between their Mg and Si abundances. We adopt the Si abundance from the Si II lines, because it is consistent with the level of overabundance seen in Mg.

The sulphur abundance is very uncertain because it relies on a single line at 912.28 nm, which is contaminated by a telluric absorption feature; we estimate an error of 0.3 dex. Assuming that our process of dividing out the telluric feature has been successful, sulphur is found to be overabundant by about 0.4 dex with respect to iron, in line with Mg. The general behaviour of S in metal-poor stars is that sulphur is enhanced over iron, [S/Fe] > 0 (François 1987, 1988; Israelian & Rebolo 2001; Chen et al. 2002). The data at very low metallicity is still rather limited, hence we cannot comment here on any general trend with declining metallicity.

Ca and Ti exhibit "normal" overabundances with respect to iron, of the order of 0.3 dex.

4.3. The odd-Z elements

The sodium abundance was obtained from the NaI D resonance lines, and displays a marked overabundance with respect to iron of ∼0.5 dex. The aluminium abundance was derived from the resonance line at 394.4 nm, and Al is underabundant by ∼−0.7 dex with respect to iron.

These abundances are the LTE values; no NLTE corrections, as prescribed by Baumüller & Gehren (1997) and Baumüller et al. (1998), have been applied. The prescribed NLTE corrections for $T_{\rm eff}$ = 6500 K, log g = 4.0, [Fe/H] = −3.0 are −0.11 and +0.65 for Na and Al, respectively. If we assume these values to apply for our lower-gravity star, then Al follows iron while Na will still be overabundant by ∼0.4 dex with respect to iron, reminiscent of the similar, but vastly larger overabundance of Na in CS 22949–037 (Depagne et al. 2002).

4.4. The iron-peak elements

Our derived Fe abundance places CS 29497–030 among the very metal-poor stars, with [Fe/H] < −2.0. Our Fe abundance and surface gravity were independently checked by Andreas Korn, who found [Fe/H] = –2.71, log g = 3.40 in LTE, using a separate set of atmospheric models and line data, and [Fe/H] = –2.59, log g = 3.65 in NLTE.

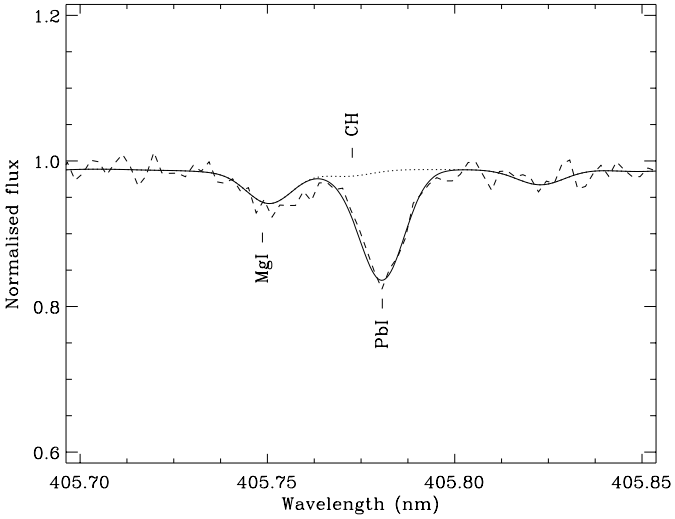

Fig. 5. The Pb I 405.7 nm line. The dotted line shows the (small) contribution of the CH line blend (for [O/Fe] = +1.67).

Mn and Cr show a slight underabundance of ∼0.2 dex compared to iron. This is in line with the general decrease of the ratios of these elements relative to iron initially found by McWilliam et al. (1995) and confirmed by other authors (Ryan et al. 1996; Carretta et al. 2002; François et al. 2003). Cobalt, on the other hand, shows a slight overabundance with respect to iron. This behaviour has also been seen before in very metal-poor stars (McWilliam et al. 1995; Ryan et al. 1996; François et al. 2003).

4.5. The neutron-capture elements

All the *s*-process elements in CS 29497–030 exhibit overabundances with respect to iron, and the heavy *s*-process elements (hs: Ba, Ce, La, Nd) are more overabundant than the lighter *s*-process elements (ls: Sr, Y, Zr). The Pb abundance was derived from the 405.7 nm line shown in Fig. 5. The line data has been taken from van Eck et al. (2003); we have included the hyperfine splitting and isotopic shifts as given in van Eck et al. (2003). We also detect the PbI 368.3 nm and 406.2 nm lines in our spectra, from which we derive abundances that are consistent with the 405.7 nm line. The derived abundance of Pb is very high, about 3.5 dex relative to iron, and also very high compared to those of Ba, La, Ce, and Nd (e.g., [Pb/Ba] = +1.38).

The Sr abundance was determined from the Sr II resonance lines, which are quite strong (equivalent widths of the order of 10 pm (where 1 pm = 10^{-12} m). We detected seven BaII lines, including the resonance lines at 455.40 nm and 493.40 nm. In our analysis of Ba, we have adopted the hyperfine splitting provided by McWilliam et al. (1995). We checked the effect of adopting either the solar-system total abundance or the solar-system *s*-process isotopic fraction, and found that the derived abundance does not change. For our final determination we used only the weaker lines, like the 585 nm line shown in Fig. 6, since the stronger lines are clearly affected by saturation. Note that increasing the microturbulence by only 0.5 km s^{-1} achieves a concordance between Ba abundances derived from

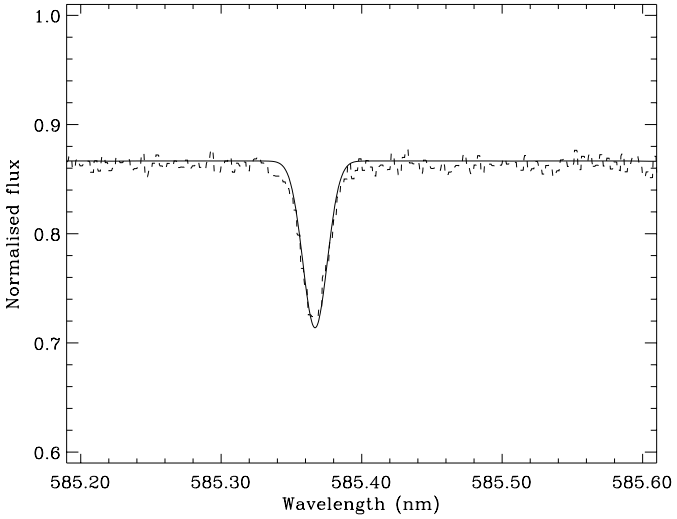

Fig. 6. The Ba II 585 nm line.

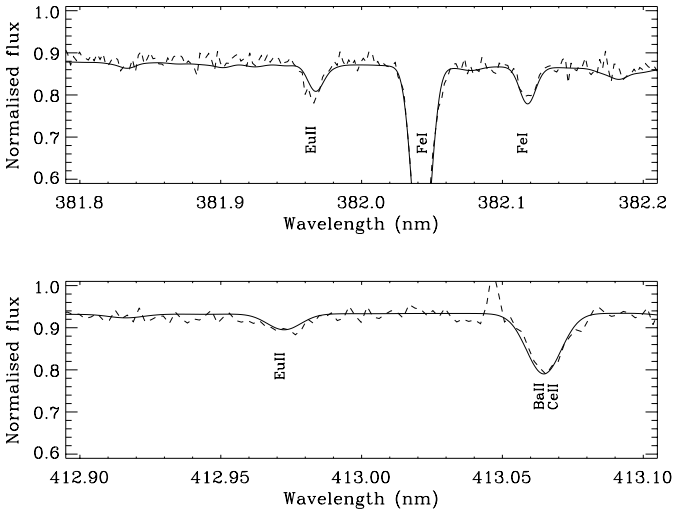

Fig. 7. Two Eu II lines.

weak and strong lines. We thus believe our Ba abundance to be very robust.

La, Ce, and Nd abundances were determined using spectrum synthesis. We have not used any hyperfine splitting for the La, Ce, Nd, and Y lines, since they are weak and the abundances are not expected to be affected by hyperfine splitting (McWilliam et al. 1995). A total of six Eu II lines are detected in our spectra; two such lines are shown in Fig. 7. We have checked, using the hyperfine splitting provided by Kurucz (1993), that the derived abundance is insensitive to the use of hyperfine splitting. The abundance listed in Table 4 has been obtained using the gf values from Lawler et al. (2001), and without hyperfine splitting.

Table 4. Elemental abundances for CS 29497–030.

Species	$A(X)_\odot$	[X/H]	[X/Fe]	σ	n
Li I	1.10	<0.00	<2.7	···	···
C I	8.52	−0.01	2.69	0.24	22
CH	···	−0.32	2.38	···	···
CN	7.92	−0.82	1.88	···	···
O I	8.74	−1.03	1.67	0.1	3
NaI	6.33	−2.18	0.52	0.15	2
MgI	7.58	−2.16	0.54	0.21	4
MgII	···	−2.06	0.64	···	1
Al I	6.47	−3.37	−0.67	···	1
Si I	7.55	−2.75	−0.05	···	1
Si II	7.55	−2.10	0.60	···	2
S I	7.33	−2.30	0.40	···	1
K I	5.12	<−2.00	<0.7	···	···
Ca I	6.36	−2.37	0.33	0.17	9
Sc II	3.17	−2.40	0.30	0.05	3
Ti I	5.02	−2.54	0.16	···	1
Ti II	···	−2.41	0.29	0.28	19
Cr I	5.67	−2.87	−0.17	0.12	6
Cr II	···	−2.75	−0.05	0.07	4
Mn I	5.39	−2.89	−0.19	0.28	3
Mn II	···	−2.87	−0.17	0.00	2
Fe I	7.50	−2.77	−0.07	0.14	55
Fe II	···	−2.70	−0.00	0.10	5
Co I	4.92	−2.28	0.42	0.10	2
Ni I	6.25	−2.91	−0.21	0.22	11
Zn I	4.60	<−2.80	<−0.10	···	···
Sr II	2.97	−1.86	0.84	0.05	2
Y II	2.24	−1.99	0.71	0.07	5
Zr II	2.60	−1.27	1.43	0.15	3
Ba II	2.13	−0.53	2.17	0.25	6
La II	1.17	−0.60	2.10	0.10	11
Ce II	1.58	−0.56	2.14	0.17	4
Nd II	1.50	−0.85	1.85	0.10	8
Eu II	0.51	−1.26	1.44	0.15	6
Pb I	1.95	0.85	3.55	···	1
$^{12}C/^{13}C$			>10		

5. Discussion

5.1. s-process nucleosynthesis in metal-poor stars

The most likely site for the the *s*-process is the inter-shell region of a thermally pulsating AGB star, provided a suitable neutron source is active. Until recently it was believed that stars of zero or extremely low metallicity did not experience the TP-AGB phase (Fujimoto et al. 1984). In contrast, Chieffi et al. (2001) have recently shown that zero-metallicity stars *do* undergo thermal pulses, although by a somewhat different mechanism, at least for stars in the range $4\ M_\odot \leq M \leq 6\ M_\odot$. These results have been independently confirmed by Siess et al. (2002).

Our present understanding of the behaviour of *s*-process nucleosynthesis has been reviewed by Busso et al. (1999). There is a general consensus that the neutron source is the reaction $^{13}C(\alpha, n)^{16}O$. In order to activate it, a partial mixing of protons into the C-rich layer is required. The hydrogen is burned through $^{12}C(p, \gamma)^{13}N(e^+\nu)^{13}C(p, \gamma)^{14}N$, leaving a residual ^{13}C abundance (Iben & Renzini 1982). Although the majority of workers in the field admit that this partial mixing does take place, there is no consensus on the *amount* of mixing, nor on the profile of the resulting ^{13}C *pocket*. The usual practice has

been to simply assume the amount of ^{13}C (Gallino et al. 1998; Goriely & Mowlavi 2000; Busso et al. 2001; Goriely & Siess 2001).

Zero-metal stars are a special case in that one could expect the lack of Fe seeds to prevent the operation of the *s*-process even in the presence of a suitable neutron flux. However, Goriely & Siess (2001) showed that if there is a partial mixing of protons, then the *s*-process proceeds, starting from ^{12}C, and builds all the heavy metals up to Pb and Bi. All of these authors agree on the existence of a large enhancement of lead with respect to the nearby second-peak *s*-process elements (Ba, La, Ce, Nd). This is a consequence of the large neutron-to-seed ratio.

Recently, Iwamoto et al. (2003) have proposed a new *s*-process paradigm, in which the abundances of the neutron-capture elements result from only one (or at most a few) neutron exposures. They find that, in models of metallicity less than [Fe/H] = –2.5, the helium convective shell penetrates the H-rich layers, allowing proton mixing to occur. In their scenario, they achieve a high neutron flux, and almost all of the *s*-process elements (except Pb) are made in the first neutron irradiation. The abundance of Pb is more sensitive to the number of pulses. From their models they were able to explain the observed abundance patterns of LP 625-44 and LP 706-7, which have Pb/Ba $\sim$ +1.0 and could not be easily explained by standard partial-mixing scenarios (Gallino et al. 1998; Goriely & Mowlavi 2000; Busso et al. 2001; Goriely & Siess 2001).

5.2. The evolutionary status of CS 29497–030

Compared to most other very metal–poor stars, CS 29497–030 stands out for its high effective temperature. There is little doubt that the star is indeed hotter than most other metal–poor stars that have been analysed to date, because we detect the Mg II 448 nm doublet. This immediately poses an age problem, because the star is considerably hotter than the main-sequence turnoff (TO) of theoretical isochrones of age 10 Gyr and comparable metallicity (Z = 0.0001; Girardi et al. 2002). Our derived gravity also implies that the star is more luminous than the TO, however it is not sufficiently luminous to be assigned to the horizontal-branch stage of evolution. Its evolutionary status thus appears to be a puzzle.

It is likely that the anomalous position of CS 29497–030 in the (log T, log g) plane is due to its binary nature and past accretion history. Given that the Halo TO is considerably redder than this star, it is legitimate to call it a "Halo Blue Straggler." It was in fact expected that some of the BMP stars (which this object has been identified as) are indeed bona fide Blue Stragglers. It is interesting to notice that one of the principal conclusions of the radial velocity investigation of Preston & Sneden (2000) was that many candidate BMP stars are indeed halo binary blue stragglers formed by mass transfer rather than merger.

We note that the LiI 670.8 nm doublet is not detected in our spectra. This is consistent with the identification of CS 29497–030 as a blue straggler, since such stars are observed to be highly Li-depleted (Glaspey et al. 1994). Ryan et al. (2002) identified several ultra Li-depleted halo stars that exhibit large projected rotational velocities, which prompted them to suggest that these stars had experienced previous transfer of mass and angular momentum from a massive companion. Preston & Sneden (2000) obtained a rather large rotational velocity ($v \sin i$ = 12 km s^{-1}) for CS 29497–030. All our spectra, at both observed epochs, show lines with a FWHM of $\sim$9.55 km s^{-1}, which is larger than the $\sim$7 km s^{-1} expected from our instrumental resolution. If interpreted as due to rotation, the excess broadening would be of the order of $\sim$6.5 km s^{-1}. Such rotational velocities are unexpected for old halo stars and hence provide evidence that the surviving star of the binary system has been significantly spun up due to mass transfer. In fact this is far larger than that corresponding to synchronous rotation of the star in its 342-day circular orbi, which would be below 0.5 km s^{-1}.

5.3. The chemical history of CS 29497–030

The observed abundance pattern of this star strongly suggests the occurrence of mass transfer in the binary system during the AGB phase of the companion, which is detected through the present orbital motion of the surviving member (but not unambigously from the photometry or the spectroscopy). The existing observations are, however, consistent with the hypothesis that the companion is presently a white dwarf. The period of about one year implies a rather wide separation, hence mass transfer must have occurred through a stellar wind (or superwind) phase on the AGB, and is likely to have happened during the thermally pulsating episodes experienced by the companion. In this scenario, it is the third dredge-up that is responsible for bringing to the surface of the companion the carbon that is freshly produced in the He-burning shell, as well as the *s*-process elements.

The pattern of neutron-capture elements in CS 29497–030 seems to show a pure *s*-process signature, as suggested in Fig. 8 which compares the abundance pattern in the star with the main *s*-process pattern from Arlandini et al. (1999). All the heavy elements above Z = 40 fit the pattern rather well, except for Pb.

In Fig. 9 we compare the abundance pattern of CS 29497–030 to the surface abundances of a model AGB star with Z = 0.001 after 50 thermal pulses, taken from Goriely & Mowlavi (2000). The overall agreement for CS 31062–050 is better than in Fig. 8. For both stars the large Pb overabundance is reproduced within a factor of 3. It is, however, quite striking to note the large underabundance of Sr, Y, and Zr compared to both the models and the main solar system *s*-component. Several known *s*-process-rich, very metal-poor stars have high ratios (more than 1.0 dex) of the heavy *s*-process elements (hs: La, Ce, Nd) relative to the lighter *s*-process elements (ls: Sr, Y, Zr) (Hill et al. 2000). CS 29497–030 has [Ba/Eu] = +0.73, and [hs/ls] = +1.02, which is quite similar to other *s*-process-enhanced, very metal-poor stars.

In Fig. 10 we compare the observed [X/Fe] ratios in CS 29497–030 and CS 31062–050 with the theoretical *s*-process computations of Gallino et al. (in preparation). In the case shown the AGB companion had a Main Sequence mass of 1.3 $M_{\odot}$. The accretion was modeled as occurring through

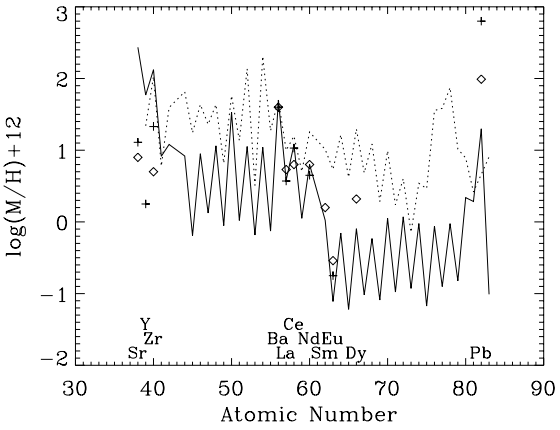

Fig. 8. Abundance patterns of *s*-process enhanced stars. The solid line indicates the main solar-system *s*-process component determined by Arlandini et al. (1999), while the dotted line indicates the *r*-process component. The "+" symbol indicates the abundances for CS 29497–030; the "⋄" represents CS 31062–050 (from Aoki et al. 2002b). The abundance patterns are normalised to Ba.

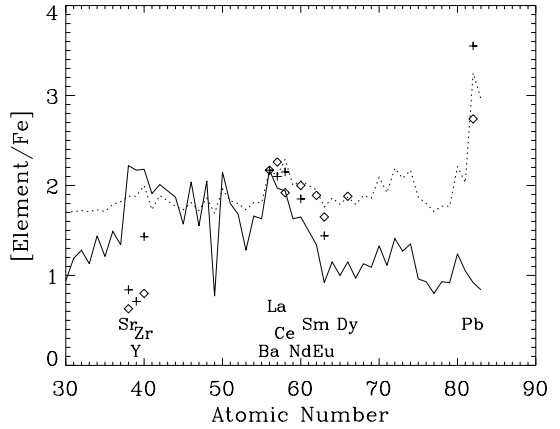

Fig. 9. Abundance patterns of *s*-process enhanced stars. The solid line indicates the surface abundance of an AGB model with solar metallicity, while the dotted line indicates the surface abundance of an AGB model with $Z = 0.001$ after 50 thermal pulses (Goriely & Mowlavi 2000). The "+" symbol indicates the abundances for CS 29497–030; the "⋄" represents CS 31062–050 (from Aoki et al. 2002b). The abundance patterns are normalised to Ba.

stellar wind, rather than Roche-Lobe overflow, which seems a reasonable assumption for such a wide system. The agreement is quite good for the heavy elements, the Zr abundance is now well reproduced; although the predicted Y and Sr remain too high. Even more interesting is that a considerable enhancement of O is predicted in the model. This arises from the $^{12}C(\alpha,\gamma)^{16}O$ reaction occurring in the He shell. Although the amount of O produced is small, at such a low metallicity it is sufficient to enhance the [O/Fe] ratio by about 0.5 dex.

In Table 5 we have summarised the data for all stars with lead detections. This table includes stars that exhibit predominantly *s*-process patterns (Aoki et al. 2001, 2002b; Johnson & Bolte 2002; Lucatello et al. 2003), and some with predominantly *r*-process patterns (Sneden et al. 1998, 2000; Travaglio et al. 2001). Some of them are known to be binaries, and some are known CH stars (van Eck et al. 2001, 2003).

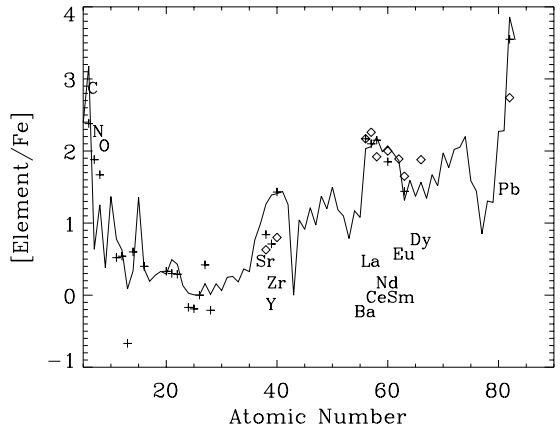

Fig. 10. Comparison between the observed abundances in CS 29497–030 ("+" symbol) and CS 31062–050, from Aoki et al. (2002b) ("⋄"), with the theoretical *s*−process nucleosynthesis computations of Gallino et al. (in preparation) for accretion from a 1.3 $M_\odot$ star in the AGB phase through stellar wind. The abundances from the AGB star are considered to be diluted by a factor of 2 by the unprocessed material of the envelope of the companion star. No normalization of abundances has been applied.

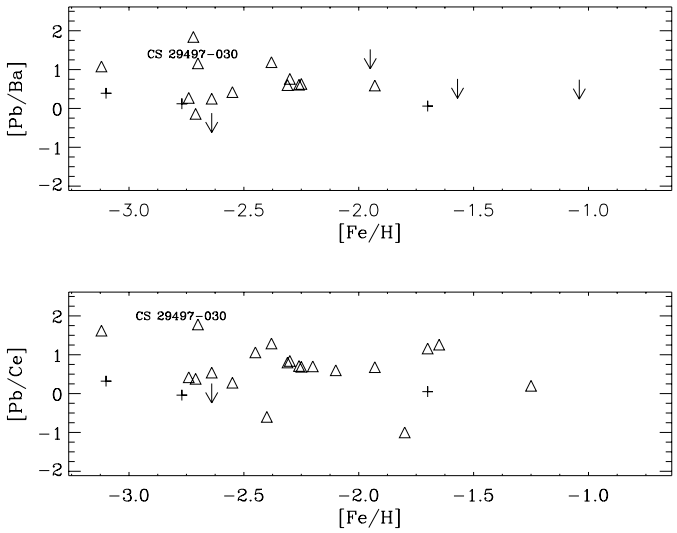

Fig. 11. [Pb/Ba] and [Pb/Ce] ratios as a function of metallicity. The data shown are taken from the list in Table 5. The three *r*-process-enhanced stars CS 22892–052, HD 1262238, and HD 115444, are plotted as crosses. Upper limits are shown as downward arrows.

In Fig. 11 we have assembled the reported [Pb/Ba] and [Pb/Ce] ratios for all the stars listed in Table 5, which summarizes results for metal-poor stars where these ratios are available. A large scatter is apparent; the *r*-process-enhanced stars CS 22892–052, HD 126238, and HD 115444 do not stand out against the others. In Fig. 12 we show [Pb/Eu] for all of the metal-poor stars for which both Pb and Eu have been measured. The crosses represent the three *r*-process-enhanced stars CS 22892–052, HD 1262238, and HD 115444. It is clear that the *r*-process-enhanced stars stand out from the others, which follow an *s*-process pattern instead. The *r*-process-enhanced stars are well below both the [Pb/Eu] ratio predicted by the metal-poor AGB models (Goriely & Mowlavi 2000) and the

Table 5. Summary of available data for lead (Pb) in metal-poor stars.

Object	$T_{\rm eff}$/log g	[Fe/H]	[C/Fe]	[Ba/Fe]	[Ce/Fe]	[Pb/Fe]	[Eu/Fe]	Binary	Period (days)
CS 22183–015[1]	5200,2.5	−3.12	2.2[2]	2.09	1.55	3.17	1.39	···	···
CS 22880–074[3]	5850,3.8	−1.93	1.3	1.31	1.22	1.9	0.5	no	···
CS 22892–052[4]	4710,1.5	−3.1	1.0[5]	0.96	1.03	1.35	1.66	···	···
CS 22898–027[3]	6250,3.7	−2.26	2.2	2.23	2.13	2.84	1.88	no	···
CS 22942–019[3]	5000,2.4	−2.64	2.0	1.92	1.54	≤1.6	0.79	yes	2800
CS 29497–030[6]	6650,3.5	−2.70	2.38	2.17	2.14	3.55	1.44	yes	342
CS 29526–110[3]	6500,3.2	−2.38	2.2	2.11	2.01	3.3	1.73	yes	···
CS 30301–015[3]	4750,0.8	−2.64	1.6	1.45	1.16	1.7	0.2	···	···
CS 31062–012[3]	6250,4.5	−2.55	2.1	1.98	2.12	2.4	1.62	···	···
CS 31062–050[3]	5600,3.0	−2.31	2.0	2.30	2.10	2.9	1.84	···	···
LP 625–44[7]	5500,2.8	−2.71	2.1	2.74	2.22	2.6	1.72	yes	···
LP 706–7[7]	6000,3.8	−2.74	2.15	2.01	1.86	2.28	1.40	no	···
HD 26 [8]	5170,2.2	−1.25	···	···	1.7	1.9	···	···	···
HD 2665[9]	5061,2.35[10]	−1.95[10]	−0.13[10]	−0.32	···	<1.	···	···	···
HD 21581[9]	4978,2.29[10]	−1.57[10]	−0.25[10]	−0.06	···	<0.5	···	···	···
HD 115444[11]	4750,1.7[11]	−2.77[11]	−0.11[12]	0.18[12]	0.34[12]	0.30[11]	0.85[12]	···	···
HD 126238[13]	4979,2.5[14]	−1.7[14]	···	−0.11	−0.1	−0.05[13]	0.17[14]	···	···
HD 187861[15]	5320,2.3	−1.65	1.89	···	1.14	2.40	···	···	···
HD 189711[16]	3500,0.5	−1.8	···	···	1.7	0.7	···	···	···
HD 196944[3]	5250,1.8	−2.25	1.2	1.07	1.01	1.7	0.17	···	···
HD 196944[7]	5250,1.7	−2.45	1.32	···	1.09	2.15	···	···	···
HD 198269[16]	4800,1.3	−2.2	···	···	1.5	2.2	···	···	···
HD 201626[16]	5190,2.25	−2.1	···	···	1.8	2.4	···	···	···
HD 201891[9]	5991,4.30[10]	−1.04[10]	0.11[10]	−0.04	···	<0.5	···	···	···
HD 224959[15]	5200,2.3	−1.7	1.95	···	1.39	2.55	···	···	···
HD 23439A[9]	5140,4.48[10]	−0.99[10]	0.09[10]	0.21	···	0.6	···	···	···
HE 0024-2523[17]	6625,4.3	−2.72	2.6	1.46	···	3.3	<1.1	yes	3.14
HE 2148-1247[18]	6380,3.9	−2.3	1.91	2.36	2.28	3.12	···	yes	···
V Ari[8]	3580,-0.2	−2.4	···	···	1.6	1.0	···	···	···

[1] Johnson & Bolte (2002), [2] Norris et al. (1997), [3] Aoki et al. (2002b), [4] Sneden et al. (2000), [5] Barbuy et al. (1997), [6] Present work, [7] Aoki et al. (2001), [8] van Eck et al. (2003), [9] Travaglio et al. (2001), [10] Gratton et al. (2000), [11] Sneden et al. (1998), [12] Westin et al. (2000), [13] Cowan et al. (1996), [14] Gratton & Sneden (1994), [15] van Eck et al. (2001), [16] van Eck et al. (2003), [17] Lucatello et al. (2003), [18] Cohen et al. (2003).

solar *s*-process main component pattern (Arlandini et al. 1999), while all the stars that are close to the horizontal lines also show enhanced *s*-process elements. CS 29497–030 exhibits a very high [Pb/Eu] ratio (indicated by an arrow in Fig. 12).

In the bottom panel of Fig. 12, we show [Ba/Eu] as a function of metallicity for all the stars in Table 5 for which Ba was measured, as well as for the stars of McWilliam (1998) (filled symbols) and for CS 31082–001 from Hill et al. (2002), plotted as an asterisk. In this figure the *r*-process-enhanced stars stand out with respect to the *s*-process pattern stars. The comparison with the "normal" halo stars of McWilliam (1998), i.e. those not enhanced in neutron-capture elements, suggests that these stars follow the *r*-process pattern. The sole exception is CS 22947–187, a carbon-enhanced, metal-poor star that falls in the regime occupied by the *s*-process-enhanced stars. It is interesting to note that CS 31082–001 falls in the middle between the *s*-process and *r*-process-enhanced stars.

CS 29497–030 also exhibits a conspicuously large nitrogen overabundance. In terms of [C/N], however, the star is not exceptional among the Pb stars, which span the range $-0.1 \leq$ [C/N] ≤ 1.3, and in fact has the same [C/N] as HE 0024–2523 (Lucatello et al. 2003). The possible origin of the nitrogen could be a massive AGB companion, which can produce N through the Hot Bottom Burning (HBB) process. However, existing AGB models predict that the N abundance should be higher than that of C when HBB is responsible for its production (Siess et al. 2002). Furthermore, the high *s*-process abundances observed in the Pb-rich stars cannot be obtained by this scenario. Another possible scenario that can produce C and N is via hot dredge-up (Herwig 2002). This is a simultaneous action of H-burning and third dredge-up. Herwig (2002) discusses models that are able to produce C and N with C > N, however, the *s*-process elements cannot be produced by this approach. Goriely & Siess (2001), by forcing extra mixing and initial pollution of C from the core He-burning regions, are able to solve the problem. However, these calculations are still in the preliminary stage.

The oxygen abundance of CS 29497–030 appears exceptionally high, both with respect to most other metal-poor stars (Israelian et al. 2001; Depagne et al. 2002; Meléndez & Barbuy 2002; Nissen et al. 2002; Barbuy et al. 2003), and with respect to HE 0024–2523 (Lucatello et al. 2003). On the one hand

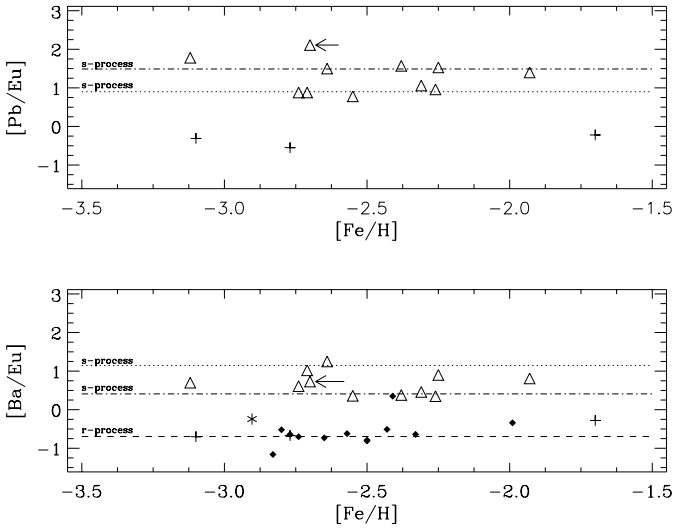

Fig. 12. [Pb/Eu] and [Ba/Eu] ratios, as a function of metallicity, for the data in Table 5; the same symbols are used as in Fig. 11. CS 29497–030 is identified by an arrow. Filled symbols are data from McWilliam (1998), the asterisk is CS 31082–001, from Hill et al. (2002). The dotted line corresponds to the solar *s*-process main component, while the dashed line corresponds to the inferred solar *r*-process value (Arlandini et al. 1999). The dash-dotted line represents the surface abundance of an AGB model with $Z = 0.001$ after 50 thermal pulses (Goriely & Mowlavi 2000).

it is true that some intermediate-mass stars may indeed produce sizeable amounts of oxygen (Marigo 2001), and perhaps at least a part of the oxygen we observe has been dumped on the surface of the star by the same process that contributed carbon and nitrogen. On the other hand, if we assume the O abundance is *intrinsic*, and not *photospheric*, then the total *metal* abundance Z of CS 29497–030 is not very low, which implies an even younger age and further exacerbates the age problem noted above. In this case it is also difficult to explain why the observed iron abundance is so low.

Inspection of Fig. 11 suggests that the observed [Pb/Ba] ratios for metal-poor stars exhibit scatter in excess of that due to observational errors. It is not clear yet whether this establishes that there is a range of operating conditions for the *s*-process at low metallicities.

6. Conclusions

The number of lead-rich, extremely metal-poor stars has now grown up to 25. Collectively, they demonstrate unequivocally that the *s*-process may already operate even at very low metallicities, and that its occurrence is not very rare. This also suggests that mixing of protons into the C-rich layers in low metallicity stars does indeed occur, at least in some cases, and that this has been experienced by the companion of CS 29497–030. Different ^{13}C profiles and stellar masses will result in different abundance patterns, as shown by Busso et al. (2001); it is therefore possible that a suitable choice of both will reproduce the observed heavy element pattern for CS 29497–030 and other stars like it.

Whether or not these nucleosynthesis products have an impact on the early chemical evolution of the Galaxy is still an open question. It depends crucially on how many C- and *s*-process-element producing stars of zero- or extremely low metallicity existed during the first and second generations of star formation, and on how efficiently their products were mixed into the ISM. Burris et al. (2000) provided evidence that the *s*-process becomes globally important beginning at [Fe/H] = ∼−2.7; however, the extremely metal-poor star CS 22183–015 displays an almost pure *s*-process-element pattern already at [Fe/H] = –3.12 (Johnson & Bolte 2002). Whether stars such as these are the exception or the rule at extremely low metallicity will have to be addressed, based on more complete high-resolution analyses of a larger sample of stars, in the near future.

The comparison made in Fig. 12 with "normal" halo stars suggests that most of these exhibit elemental abundance patterns that lie close to the *r*-process pattern. More data are needed to draw definitive conclusions; however the presently available observations suggest that the *r*-only hypothesis of Truran (1981) as the *standard* assumption is questionable, and chemical evolution models ought to take into account a mixture of *s*- and *r*-processes for the production of the heavy metals at arbitrarily low metallicity. High-resolution analyses of a larger number of very metal-poor stars will allow for better constraints on the relative contributions of the two processes in the early Galaxy.

All of the lead-rich stars with *s*-process enhancement show large carbon abundances, like the classical CH stars. The fact that many of them appear to be members of binary systems emphasizes the analogy. A detailed comparison of nitrogen abundances for these stars could be quite important, in order to set limits on the likely masses of presumed AGB companions, which could have experienced different mixing, mass-loss, and nucleosynthesis episodes in the course of their evolution.

Our analysis has shown that CS 29497–030 is an extreme case of a lead-rich, very metal-poor star. Its binary nature suggests that the large enhancement of neutron-capture elements which follow an *s*-process pattern, as well as the large enhancement of C and N, is in fact due to mass transfer from an intermediate-mass companion during its AGB phase. The very low iron abundance implies that *s*-process sources are active at quite early times in Galactic history. The apparently large O abundance, if real, is not easy to explain, nor is the overabundance of Na which recalls the similar, but far more dramatic enhancement of Na in CS 22949–037 (Depagne et al. 2002). The comparison with other lead stars shows a sizeable scatter in abundance ratios like [Pb/Ba] and [Pb/Ce]. Although the observational error alone cannot be absolutely excluded as the source of the observed scatter, the possibility exists that the scatter is real and due to different physical conditions in the operation of the early *s*-process. Our preliminary finding of a relatively large axial rotational velocity for CS 29397–030, the high $T_{\rm eff}$ of the star, and the lack of detectable Li, suggest that CS 29397–030 has been "spun up" as the result of mass transfer and should be classified as a halo blue straggler, similar in many respects to the stars described by Ryan et al. (2002). Detailed analyses of other such stars are certain to be illuminating.

Acknowledgements. We are grateful to A. Korn for performing the NLTE computations for Fe. Special thanks are due to R. Gallino for illuminating discussions on *s*-process nucleosynthesis and for providing us the results of his computations in advance of publication. We also wish to acknowledge helpful discussions with H. Schlattl, L. Girardi and S. Zaggia. Thanks to F. Herwig for his input on the issue of nitrogen. Finally we thank the referee G. Preston whose comments contributed to considerably improve this paper. This research received support from the italian MIUR COFIN2002 grant 2002028935_003. BA and JA thank the Carlsberg Foundation and the Swedish and Danish Natural Science Research Councils for financial support for this work. T.C.B acknowledges partial support from grants AST 00-98508 and AST 00-98549, awarded by the U.S. National Science Foundation. This publication makes use of data products from the 2MASS All Sky Survey, which is a joint project of the University of Massachusetts and the Infrared Processing and Analysis Center/California Institute of Technology, funded by the National Aeronautics and Space Administration and the National Science Foundation.

References

Abia, C., Domínguez, I., Straniero, O., et al. 2001, ApJ, 557, 126
Alonso, A., Arribas, S., & Martínez-Roger, C. 1996, A&A, 313, 873
Aoki, W., Norris, J. E., Ryan, S. G., Beers, T. C., & Ando, H. 2000, ApJ, 536, L97
Aoki, W., Ryan, S. G., Norris, J. E., et al. 2001, ApJ, 561, 346
Aoki, W., Norris, J. E., Ryan, S. G., Beers, T. C., & Ando, H. 2002, ApJ, 567, 1166
Aoki, W., Ryan, S. G., Norris, J. E., et al. 2002, ApJ, 580, 1149
Aoki, W., Norris, J. E., Ryan, S. G., Beers, T. C., & Ando, H. 2002, ApJ, 576, L141
Arlandini, C., Käppeler, F., Wisshak, K., et al. 1999, ApJ, 525, 886
Arribas, S., & Roger, C. M. 1987, A&AS, 70, 303
Barbuy, B., Ortolani, S., & Bica, E. 1994, A&A, 285, 871
Barbuy, B., Cayrel, R., Spite, M., et al. 1997, A&A, 317, L63
Barbuy, B., Meléndez, J., Spite, M., et al. 2003, ApJ, 588, 1072
Baumüller, D., & Gehren, T. 1997, A&A, 325, 1088
Baumüller, D., Butler, K., & Gehren, T. 1998, A&A, 338, 637
Beers, T. C. 1999a, The Third Stromlo Symposium: The Galactic Halo, ASP Conf. Ser., 165, 202
Beers, T. C. 1999b, Ap&SS, 265, 547
Beers, T. C., Preston, G. W., & Shectman, S. A. 1985, AJ, 90, 2089
Beers, T. C., Preston, G. W., & Shectman, S. A. 1992, AJ, 103, 1987
Beers, T. C., Flynn, C., Rossi, S., et al. 2003, AJ, in preparation
Bessell, M. S. 1983, PASP, 95, 480
Bessell, M. S., & Brett, J. M. 1988, PASP, 100, 1134
Biémont, E., Baudoux, M., Kurucz, R. L., Ansbacher, W., & Pinnington, E. H. 1991, A&A, 249, 539
Bonifacio, P., Molaro, P., Beers, T. C., & Vladilo, G. 1998, A&A, 332, 672
Burris, D. L., Pilachowski, C. A., Armandroff, T. E., et al. 2000, ApJ, 544, 302
Busso, M., Gallino, R., Lambert, D. L., Travaglio, C., & Smith, V. V. 2001, ApJ, 557, 802
Busso, M., Gallino, R., & Wasserburg, G. J. 1999, ARA&A, 37, 239
Carpenter, J. M. 2001, AJ, 121, 2851
Carretta, E., Gratton, R. G., & Sneden, C. 2000, A&A, 356, 238
Carretta, E., Gratton, R., Cohen, J. G., Beers, T. C., & Christlieb, N. 2002, AJ, 124, 481
Cayrel, R., Hill, V., Beers, T. C., et al. 2001, Nature, 409, 691
Cayrel, R., Andersen, J., Barbuy, B., et al. 2001, New Astron. Rev., 45(8), 533
Chen, Y. Q., Nissen, P. E., Zhao, G., & Asplund, M. 2002, A&A, 390, 225
Chieffi, A., Domínguez, I., Limongi, M., & Straniero, O. 2001, ApJ, 554, 1159
Christlieb, N., Reimers, D., Wisotzki, L., et al. 2000, The First Stars. Proceedings of the MPA/ESO Workshop held at Garching, Germany, 4–6 August 1999, ed. A. Weiss, T. G. Abel, & V. Hill (Springer), 49
Cohen, J. G., Christlieb, N., Qian, Y.-Z., & Wasserburg, G. J. 2003 [astro-ph/0301460]
Cowan, J. J., Sneden, C., Truran, J. W., & Burris, D. L. 1996, ApJ, 460, L115
Cutri, R. M., Skrutskie, M. F., Van Dyk, S., et al. 2003, Explanatory Supplement to the 2MASS All Sky Data Release, http://www.ipac.caltech.edu/2mass/releases/allsky/doc/explsup.html
Dekker, H., D'Odorico, S., Kaufer, A., Delabre, B., & Kotzlowski, H. 2000, Proc. SPIE, 4008, 534
Depagne, E., Hill, V., Spite, M., et al. 2002, A&A, 390, 187
Elias, J. H., Frogel, J. A., Matthews, K., & Neugebauer, G. 1982, AJ, 87, 1029
François, P. 1987, A&A, 176, 294
François, P. 1988, A&A, 195, 226
François, P., Depagne, E., Hill, V., et al. 2003, A&A, 403, 1105
Frogel, J. A., Persson, S. E., Matthews, K., & Aaronson, M. 1978, ApJ, 220, 75
Fujimoto, M. Y., Iben, I., Chieffi, A., & Tornambé, A. 1984, ApJ, 287, 749
Gallino, R., Arlandini, C., Busso, M., et al. 1998, ApJ, 497, 388
García López, R. J., Israelian, G., Rebolo, R., et al. 2001, New Astron. Rev., 45, 519
Gilroy, K. K., Sneden, C., Pilachowski, C. A., & Cowan, J. J. 1988, ApJ, 327, 298
Girardi, L., Bertelli, G., Bressan, A., et al. 2002, A&A, 391, 195
Glaspey, J. W., Pritchet, C. J., & Stetson, P. B. 1994, AJ, 108, 271
Goriely, S., & Mowlavi, N. 2000, A&A, 362, 599
Goriely, S., & Siess, L. 2001, A&A, 378, L25
Gratton, R. G., Sneden, C., Carretta, E., & Bragaglia, A. 2000, A&A, 354, 169
Gratton, R. G., Carretta, E., Eriksson, K., & Gustafsson, B. 1999, A&A, 350, 955
Gratton, R. G., & Sneden, C. 1994, A&A, 287, 927
Hannaford, P., Lowe, R. M., Grevesse, N., Biemont, E., & Whaling, W. 1982, ApJ, 261, 736
Herwig, F. 2002, CNO in the Universe, ed. C. Charbonnel, D. Schaerer, & G. Meynet, ASP Conf. Ser. [astro-ph/0212366]
Hill, V., Barbuy, B., Spite, M., et al. 2000, A&A, 353, 557
Hill, V., Plez, B., Cayrel, R., et al. 2002, A&A, 387, 560
Iben, I., & Renzini, A. 1982, ApJ, 263, L23
Israelian, G., & Rebolo, R. 2001, ApJ, 557, L43
Israelian, G., Rebolo, R., García López, R. J., et al. 2001, ApJ, 551, 833
Iwamoto, N., Kajino, T., Mathews, G. J., et al. 2003, J. Nucl. Sci. Technol., in press [astro-ph/0203180]
Johnson, J. A., & Bolte, M. 2002, ApJ, 579, L87
Kinman, T., & Castelli, F. 2002, A&A, 391, 1039
Kiselman, D. 2001, New Astron. Rev., 45, 559
Kiselman, D. 1991, A&A, 245, L9
Kupka, F., Piskunov, N. E., Ryabchikova, T. A., Stempels, H. C., & Weiss, W. W. 1999, A&AS, 138, 119
Kurucz, R. L. 1993, CD-ROM, 15
Lucatello, S., Gratton, R., Cohen, J. G., et al. 2003, AJ, 125, 875

Lawler, J. E., Wickliffe, M. E., & Den Hartog, E. A. 2001, ApJ, 563, 1075
Marigo, P. 2001, A&A, 370, 194
Martin, W. C., Fuhr, J. R., Kelleher, D. E., et al. 2002, NIST Atomic Spectra Database, version 2.0
McClure, R. D. 1990, ApJ, 352, 709
McClure, R. D. 1997, PASP, 109, 536
McWilliam, A. 1998, AJ, 115, 1640
McWilliam, A., Preston, G. W., Sneden, C., & Searle, L. 1995, AJ, 109, 2757
Meléndez, J., & Barbuy, B. 2002, ApJ, 575, 474
Nissen, P., Chen, Y., Asplund, M., & Pettini, M. 2002, Modelling of stellar Atmospheres., IAU Symp. 210, ASP Conf. Ser., to appear
Nissen, P. E., Primas, F., Asplund, M., & Lambert, D. L. 2002, A&A, 390, 235
Norris, J. E., Ryan, S. G., & Beers, T. C. 1997, ApJ, 488, 350
Norris, J. E., Ryan, S. G., & Beers, T. C. 1997, ApJ, 489, L169
Preston, G. W., & Sneden, C. 2000, AJ, 120, 1014
Preston, G. W., Shectman, S. A., & Beers, T. C. 1991a, ApJS, 76, 1001
Preston, G. W., Shectman, S. A., & Beers, T. C. 1991b, ApJ, 375, 121
Preston, G. W., Beers, T. C., & Shectman, S. A. 1994, AJ, 108, 538
Ryan, S. G., Norris, J. E., & Beers, T. C. 1996, ApJ, 471, 254
Ryan, S. G., Gregory, S. G., Kolb, U., Beers, T. C., & Kajino, T. 2002, ApJ, 571, 501
Schlegel, D. J., Finkbeiner, D. P., & Davis, M. 1998,ApJ, 500, 525
Siess, L., Livio, M., & Lattanzio, J. 2002, ApJ, 570, 329
Sivarani, T., et al. 2002, Talk given at the meeting on Early Galactic Chemical Evolution with UVES, held at ESO Garching on 29–30th November 2002 [astro-ph/0212406]
Spite, M., & Spite, F. 1978, A&A, 67, 23
Sneden, C., Cowan, J. J., Lawler, J. E., et al. 2003, ApJ, 591, 936
Sneden, C., Preston, G. W., & Cowan, J. J. 2003, ApJ, 592, 504
Sneden, C., Cowan, J. J., Ivans, I. I., et al. 2000, ApJ, 533, L139
Sneden, C., Cowan, J. J., Burris, D. L., & Truran, J. W. 1998, ApJ, 496, 235
Sneden, C., McWilliam, A., Preston, G. W., et al. 1996, ApJ, 467, 819
Sneden, C., Preston, G. W., McWilliam, A., & Searle, L. 1994, ApJ, 431, L27
Takeda, Y. 1994, PASJ, 46, 53
Travaglio, C., Gallino, R., Busso, M., & Gratton, R. 2001, ApJ, 549, 346
Truran, J. W. 1981, A&A, 97, 391
van Eck, S., Goriely, S., Jorissen, A., & Plez, B. 2001, Nature, 412, 793
van Eck, S., Goriely, S., Jorissen, A., & Plez, B. 2003, A&A, 404, 291
Westin, J., Sneden, C., Gustafsson, B., & Cowan, J. J. 2000, ApJ, 530, 783
Wilhelm, R., Beers, T. C., Sommer-Larsen, J., et al. 1999, AJ, 117, 2329

Online Material

Table 6. Line list.

Element	λ(nm)	Low.Exc (eV)	log(gf)	EW(pm)	Ref.
C I	437.1367	7.68	−2.333	4.33	1
C I	476.6677	7.48	−2.617	1.66	1
C I	477.0026	7.48	−2.439	2.29	1
C I	477.1746	7.49	−1.866	5.50	1
C I	477.5895	7.49	−2.304	2.78	1
C I	493.2049	7.68	−1.884	4.84	1
C I	502.3839	7.95	−2.209	1.63	1
C I	505.2167	7.68	−1.648	7.47	1
C I	538.0337	7.68	−1.842	5.25	1
C I	579.3124	7.95	−2.062	1.12	1
C I	580.0602	7.95	−2.338	1.01	1
C I	600.1118	8.64	−2.061	0.28	1
C I	601.4834	8.64	−1.585	0.97	1
C I	658.7610	8.54	−1.596	3.65	1
C I	708.7836	8.647	−1.443	1.81	1
C I	709.3234	8.647	−1.697	syn	1
C I	710.0123	8.643	−1.470	1.70	1
C I	710.8930	8.640	−1.592	1.62	1
C I	711.1469	8.640	−1.086	2.96	1
C I	711.3179	8.647	−0.774	4.61	1
C I	711.6988	8.647	−0.907	4.71	1
C I	711.9657	8.643	−1.149	3.36	1
O I	777.1941	9.146	0.369	7.79	1
O I	777.4161	9.146	0.223	6.91	1
O I	777.5390	9.146	0.001	4.18	1
Na I	588.9951	0.00	0.112	10.24	6
Na I	589.5924	0.00	−0.191	7.37	6
Mg I	416.7271	4.346	−1.004	syn	1
Mg I	517.2684	2.71	−0.380	11.64	6
Mg I	518.3604	2.72	−0.158	13.13	6
Mg I	552.8405	4.34	−0.341	2.25	6
Mg II	448.1126	8.864	0.740	syn	1
Mg II	448.1325	8.864	0.590	syn	1
Al I	394.4006	0.00	−0.640	7.49	1
Al I	396.1520	0.010	−0.340	syn	1
Si I	390.5523	1.91	−1.090	8.16	1
Si II	385.6018	6.859	−0.557	syn	1
Si II	386.2595	6.858	−0.817	syn	1
S I	921.2863	6.525	0.420	syn	1

Table 6. continued.

Element	λ(nm)	Low.Exc (eV)	log(gf)	EW(pm)	Ref.
Ca I	422.6728	0.00	0.240	10.79	6
Ca I	431.8652	1.90	−0.210	.94	6
Ca I	443.4957	1.89	0.066	1.36	1
Ca I	445.4779	1.90	0.260	3.39	6
Ca I	558.8749	2.52	0.210	1.23	6
Ca I	612.2217	1.89	−0.320	.91	6
Ca I	616.2173	1.90	−0.090	2.13	6
Ca I	643.9075	2.52	0.470	.98	6
Ca I	646.2567	2.52	0.230	.59	1
Sc II	357.6340	0.01	0.007	5.12	1
Sc II	361.3829	0.02	0.416	5.95	1
Sc II	424.6822	0.31	0.240	5.68	6
Sc II	440.0389	0.605	−0.536	syn	1
Sc II	441.5557	0.595	−0.668	syn	1
Ti I	498.1731	0.84	0.500	2.4	6
Ti II	337.2800	0.01	0.270	12.77	1
Ti II	338.0279	0.05	−0.570	3.71	1
Ti II	344.4314	0.15	−0.810	4.85	1
Ti II	349.1066	0.11	−1.060	3.25	1
Ti II	350.4896	1.89	0.180	3.66	1
Ti II	351.0845	1.89	0.140	2.84	1
Ti II	359.6052	0.61	−1.220	3.34	1
Ti II	391.3468	1.12	−0.410	5.44	1
Ti II	439.5033	1.08	−0.510	6.19	1
Ti II	439.9772	1.24	−1.220	2.11	1
Ti II	441.7719	1.16	−1.230	1.61	1
Ti II	444.3794	1.08	−0.700	4.74	1
Ti II	446.8507	1.13	−0.600	4.95	1
Ti II	450.1273	1.12	−0.760	3.89	1
Ti II	453.3969	1.24	−0.540	4.78	1
Ti II	456.3761	1.22	−0.790	4.15	1
Ti II	457.1968	1.57	−0.230	4.75	1
Ti II	480.5085	2.06	−0.960	0.53	1
Ti II	518.8680	1.58	−1.050	1.19	1
Cr I	357.8684	0.00	0.409	3.75	1
Cr I	359.3481	0.00	0.307	3.78	1
Cr I	425.4332	0.00	−0.110	2.61	6
Cr I	427.4796	0.00	−0.230	2.70	6
Cr I	520.6038	0.94	0.020	0.58	6
Cr I	520.8419	0.94	0.160	1.55	6
Cr II	335.8491	2.45	−0.722	2.76	1
Cr II	336.8041	2.48	−0.319	7.07	1
Cr II	338.2675	2.45	−0.639	2.80	1
Cr II	340.8757	2.48	−0.038	5.27	1
Cr II	342.1202	2.42	−0.611	3.73	1

Table 6. continued.

Element	λ(nm)	Low.Exc (eV)	log(gf)	EW(pm)	Ref.
Mn I	403.0753	0.00	−0.480	1.58	6
Mn I	403.3062	0.00	−0.620	1.46	6
Mn I	403.4483	0.00	−0.810	2.30	6
Mn II	344.1988	1.78	−0.270	5.18	1
Mn II	348.8677	1.85	−0.860	3.20	1
Fe I	344.0606	0.00	−0.670	6.97	1
Fe I	344.0989	0.05	−0.960	7.47	1
Fe I	355.4925	2.83	0.538	2.61	1
Fe I	356.5379	0.96	−0.133	5.68	1
Fe I	360.8859	1.01	−0.100	5.86	1
Fe I	361.0159	2.81	0.176	1.40	1
Fe I	361.8768	0.99	−0.003	5.68	1
Fe I	362.1461	2.73	−0.016	2.03	1
Fe I	384.9967	1.01	−0.970	5.06	1
Fe I	385.6372	0.05	−1.290	7.16	1
Fe I	385.9911	0.00	−0.710	9.88	1
Fe I	386.5523	1.01	−0.980	4.47	1
Fe I	392.0258	0.12	−1.750	4.57	6
Fe I	400.5242	1.56	−0.610	4.67	6
Fe I	404.5812	1.48	0.280	9.26	6
Fe I	406.3594	1.56	0.070	7.77	6
Fe I	407.1738	1.61	−0.020	7.39	6
Fe I	413.2058	1.61	−0.670	3.79	6
Fe I	414.3415	3.05	−0.204	1.20	1
Fe I	414.3868	1.56	−0.460	4.48	6
Fe I	418.1755	2.83	−0.180	1.29	6
Fe I	418.7039	2.45	−0.550	1.62	6
Fe I	418.7795	2.42	−0.550	1.91	6
Fe I	419.1431	2.47	−0.730	1.28	6
Fe I	419.9095	3.05	0.250	2.76	6
Fe I	420.2029	1.48	−0.700	4.50	6
Fe I	422.7427	3.33	0.230	1.70	1
Fe I	423.3603	2.48	−0.600	1.73	6
Fe I	425.0119	2.47	−0.400	1.65	6
Fe I	425.0787	1.56	−0.714	3.63	1
Fe I	426.0474	2.40	−0.020	4.10	6
Fe I	427.1154	2.45	−0.350	2.69	6
Fe I	427.1761	1.48	−0.160	7.40	1
Fe I	438.3545	1.48	0.200	8.77	6
Fe I	440.4750	1.56	−0.140	7.08	6
Fe I	441.5123	1.61	−0.610	3.91	6
Fe I	449.4563	2.20	−1.140	0.98	6

Table 6. continued.

Element	λ(nm)	Low.Exc (eV)	log(gf)	EW(pm)	Ref.
Fe I	473.6773	3.21	−0.750	0.40	1
Fe I	489.1492	2.85	−0.110	1.56	1
Fe I	491.8994	2.87	−0.340	1.23	1
Fe I	492.0503	2.83	0.070	2.76	1
Fe I	495.7597	2.81	0.233	3.52	1
Fe I	500.6119	2.83	−0.620	0.38	1
Fe I	501.2068	0.86	−2.642	0.14	1
Fe I	504.9820	2.28	−1.360	0.36	1
Fe I	523.2940	2.94	−0.060	1.38	1
Fe I	526.6555	3.00	−0.390	0.42	1
Fe I	526.9537	0.86	−1.320	3.79	1
Fe I	532.4179	3.21	−0.240	1.30	1
Fe I	532.8039	0.92	−1.470	3.13	1
Fe I	537.1490	0.96	−1.650	2.28	1
Fe I	538.3369	4.31	0.640	0.58	1
Fe I	539.7128	0.92	−1.990	1.28	1
Fe I	540.5775	0.99	−1.840	1.28	1
Fe I	542.9697	0.96	−1.880	1.18	1
Fe I	543.4524	1.01	−2.120	0.93	1
Fe I	544.6917	0.99	−1.910	1.30	1
Fe I	558.6756	3.37	−0.140	0.52	1
Fe I	561.5644	3.33	−0.140	1.05	1
Fe II	423.3172	2.58	−1.900	3.35	1
Fe II	492.3927	2.89	−1.320	4.42	1
Fe II	501.8440	2.89	−1.220	5.43	1
Fe II	516.9033	2.89	−1.303	6.04	1
Fe II	523.4625	3.22	−2.150	0.68	2
Co I	345.3508	0.43	0.380	2.93	1
Co I	399.5302	0.923	−0.220	syn	1
Ni I	338.0566	0.42	−0.170	3.71	1
Ni I	342.3704	0.21	−0.760	4.63	1
Ni I	343.3554	0.03	−0.668	3.63	1
Ni I	347.2542	0.11	−0.810	2.90	1
Ni I	349.2954	0.11	−0.250	6.23	1
Ni I	351.0332	0.21	−0.670	3.59	1
Ni I	351.5049	0.11	−0.211	5.04	1
Ni I	356.6366	0.42	−0.236	3.40	1
Ni I	361.0461	0.11	−1.149	1.20	1
Ni I	361.9386	0.42	0.035	4.25	1
Ni I	385.8292	0.42	−0.970	2.86	6

Table 6. continued.

Element	λ(nm)	Low.Exc (eV)	log(gf)	EW(pm)	Ref.
Sr II	407.7709	0.00	0.170	11.30	1
Sr II	421.5519	0.00	−0.170	9.86	1
Y II	360.0741	0.180	0.280	syn	7
Y II	360.1919	0.104	−0.180	syn	7
Y II	361.1044	0.130	0.110	syn	7
Y II	395.0352	0.104	−0.490	syn	7
Y II	417.7529	0.409	−0.160	syn	7
Zr II	339.1982	0.16	0.463	3.85	1
Zr II	399.1152	0.758	−0.252	syn	1
Zr II	399.8954	0.559	−0.387	syn	1
Ba II	413.0645	2.722	0.560	syn	3
Ba II	455.4029	0.00	0.170	16.59	3
Ba II	493.4076	0.00	−0.150	15.26	3
Ba II	585.3668	0.60	−1.010	5.34	3
Ba II	614.1713	0.70	−0.070	10.79	3
Ba II	649.6897	0.60	−0.377	9.20	3
La II	391.6042	0.235	−0.485	syn	1
La II	392.9211	0.173	−0.297	syn	1
La II	394.9102	0.403	0.455	syn	1
La II	398.8515	0.403	0.138	syn	1
La II	399.5745	0.173	−0.094	syn	1
La II	404.2901	0.927	0.290	syn	1
La II	408.6709	0.000	−0.032	syn	1
La II	423.8374	0.40	−0.337	1.08	1
La II	442.9905	0.235	−0.366	syn	1
La II	492.0976	0.13	−0.773	0.93	1
La II	492.1776	0.24	−0.699	1.06	1

Table 6. continued.

Element	λ(nm)	Low.Exc (eV)	log(gf)	EW(pm)	Ref.
Ce II	408.3222	0.700	0.270	0.81	8
Ce II	413.3802	0.864	0.370	0.89	8
Ce II	413.7645	0.516	0.440	1.05	8
Ce II	418.6594	0.86	0.740	2.40	8
Nd II	390.1845	0.631	−0.008	syn	1
Nd II	390.5869	0.205	−0.156	syn	1
Nd II	399.1741	0.000	−0.509	syn	1
Nd II	399.4672	0.321	−0.268	syn	1
Nd II	406.1080	0.471	0.347	syn	1
Nd II	410.9071	0.064	−0.316	syn	1
Nd II	410.9448	0.321	0.184	syn	1
Nd II	445.1563	0.380	0.026	syn	1
Eu II	381.9672	0.000	0.485	syn	4
Eu II	390.7107	0.207	0.195	syn	4
Eu II	393.0499	0.207	0.270	syn	4
Eu II	397.1972	0.207	0.270	syn	4
Eu II	412.9725	0.000	0.220	syn	4
Eu II	420.5042	0.000	0.210	syn	4
Pb I	405.7807	1.32	−0.220	syn	5
Pb I	368.3462	0.969	−0.460	syn	1

(1) VALD database (as of June 2002), (2) Biémont et al. (1991), (3) McWilliam et al. (1995), (4) Lawler et al. (2001), (5) van Eck et al. (2003), (6) Martin et al. (2002) NIST, (7) Hannaford et al. (1981), (8) D.R.E.A.M. data base `www.umh.ac.be/astro/dream.shtml`.